Journal of Magnetism and Magnetic Materials 452 (2018) 90–99

Contents lists available at ScienceDirect

Journal of Magnetism and Magnetic Materials

journal homepage: www.elsevier.com/locate/jmmm

Research articles

Fe-induced enhancement of antiferromagnetic spin correlations in $Mn_{2-x}Fe_xBO_4$

N.V. Kazak [a,*], M.S. Platunov [a], Yu.V. Knyazev [a], E.M. Moshkina [a,b], S.Yu. Gavrilkin [c], O.A Bayukov [a], M.V. Gorev [a], E.I. Pogoreltsev [a], G.M. Zeer [d], S.M. Zharkov [a,d], S.G. Ovchinnikov [a]

[a] Kirensky Institute of Physics, Federal Research Center KSC SB RAS, 660036 Krasnoyarsk, Russia
[b] Siberian State University of Science and Technologies, 660014 Krasnoyarsk, Russia
[c] P.N. Lebedev Physical Institute of RAS, 119991 Moscow, Russia
[d] Siberian Federal University, 660041 Krasnoyarsk, Russia

ARTICLE INFO

Article history:
Received 26 July 2017
Received in revised form 4 December 2017
Accepted 11 December 2017
Available online 11 December 2017

Keywords:
SRO spin correlations
Spin-glass
REHAC
Magnetic frustrations

ABSTRACT

Fe substitution effect on the magnetic behavior of $Mn_{2-x}Fe_xBO_4$ (x = 0.3, 0.5, 0.7) warwickites has been investigated combining Mössbauer spectroscopy, *dc* magnetization, *ac* magnetic susceptibility, and heat capacity measurements. The Fe^{3+} ions distribution over two crystallographic nonequivalent sites is studied. The Fe introduction breaks a long-range antiferromagnetic order and leads to onset of spin-glass ground state. The antiferromagnetic short-range-order spin correlations persist up to temperatures well above T_{SG} reflecting in increasing deviations from the Curie-Weiss law, the reduced effective magnetic moment and "missing" entropy. The results are interpreted in the terms of the progressive increase of the frustration effect and the formation of spin-correlated regions.

1. Introduction

The phase transitions and magnetic properties of frustrated magnetic systems are in the focus of intense current investigations [1,2]. Magnetic frustration has been regarded as an organizing principle governing a wide range of physical phenomena in the collective behaviors of spins. Frustrations manifest themselves in a dramatic lowering of the critical temperature or complete suppression of the long-range order as well as in exotic magnetic states such as spin liquid or spin ice. Such mechanisms like the geometrical constrains, the competing magnetic interactions or the disorder in lattices can cause frustration. Geometrical spin frustration comes from the topological arrangement of the spins [3,4]. The kagome, pyrochlore and garnet structure types are most well-known and thoroughly studied [1,5,6].

The oxyborates with warwickite and ludwigite structures represent frustrated magnetic systems with a variety of interrelated magnetic phenomena [7–9]. In the ludwigite the heavy frustrations of exchange interactions between the spin ladders have been found [10]. The heterometallic warwickites with general formula $M^{2+}M'^{3+}BO_4$ (M^{2+}, M^{3+} = Mg, Sc and transition metal ions) are an example of random frustration, where the two crystallographic nonequivalent metal sites are randomly occupied by the divalent and trivalent metals [7,11,12]. The metal ions have an octahedral coordination. Four octahedra share edges with each other, generating low-dimensional ribbons propagating along *c*-axis. Each of the metal atoms in the ribbon forms a potentially frustrated triangle network if the nearest-neighbor exchange interactions are antiferromagnetic [8]. Indeed, the heterometallic warwickites show large frustration index [3] $f = |\theta|/T_{SG}$ going up to 37 (Table 1). On cooling these materials displays the spin glass transition below T_{SG}. In the intermediated temperature range the spin dynamics probed by *ac* susceptibility shows the power-law behavior $\chi \sim T^{-\alpha}$ characteristic of random exchange Heisenberg antiferromagnetic chains (REHAC) [7,8,12]. Such power-law behavior is experimentally observed for sufficiently disordered spin antiferromagnetic chains ($MgM'BO_4$ M′ = Ti, V, Cr, Fe, and $CoFeBO_4$ [7,8,12–14]). This non-trivial magnetic behavior is a direct consequence of the warwickite structure which favors both the magnetic frustration and the low dimensionality.

At present there are reports on only two homo-metallic warwickites: Fe_2BO_4 and Mn_2BO_4, exhibiting both charge ordering and long-range magnetic order [15–19]. In Mn_2BO_4 the charge ordering of the type $Mn^{2+}(2)$-$Mn^{3+}(1)$ is associated with orbital ordering (d_z^2). The last two decades the magnetic ground state of

* Corresponding author at: Physics of Magnetic Phenomena Lab, Kirensky Institute of Physics, FRC KSC SB RAS, Academgorodok 50/38, Krasnoyarsk 660036, Russia.
E-mail address: nat@iph.krasn.ru (N.V. Kazak).

https://doi.org/10.1016/j.jmmm.2017.12.037
0304-8853/

Table 1
Magnetic properties of heterometallic warwickites. The asterisk denotes the results of present work.

	$S(M^{2+})$	$S(M^{3+})$	T_{SG}, K	θ, K	T_d, K	θ/T_{SG}	Refs.
$CuFeBO_4$	1/2	5/2	12	−200	75	16.7	[22]
$NiFeBO_4$	1	5/2	12	−450	40	37.5	[22]
$CoFeBO_4$	3/2	5/2	22	−311	150	14.1	[8]
$Mn_{1.3}Fe_{0.7}BO_4$	5/2	2, 5/2	17	−228	236	13.5	*

Mn_2BO_4 was a subject of extensive studies including neutron powder diffraction study (NPD) [18]. These measurements have revealed a long-range antiferromagnetic order below T_N = 26 K that has been confirmed by the magnetization and the specific-heat measurements [19]. In addition the magnetic anisotropy with easy-axis of magnetization in *ab*-plane has been found.

While the effects of dilution by non-magnetic cations on the magnetic lattice have been extensively studied [7,8,11–14,20–22] much less is known about the effects of magnetic substitution. The exceptions are $CuFeBO_4$, $NiFeBO_4$ and $CoFeBO_4$ [8,22] which present the mixed spin systems with $S(M^{2+}) = 1/2$, 1, 3/2 and $S(M^{3+}) = 5/2$ (Table 1). To the best of our knowledge, only two works have been published so far reporting the crystal structure of $MnFeBO_4$ [23,24]. At the same time $MnFeBO_4$ warwickite is supposed to be a spin system where only one type of spin chains exist ($S(M^{2+}) = S(M^{3+}) = 5/2$). Recently, $Mn_{2-x}Fe_xBO_4$ (x = 0.3, 0.5, 0.7) warwickite system has been synthesized and characterized by X-ray diffraction and X-ray absorption spectroscopy [25]. The comparison of Mn_2BO_4 and $Mn_{2-x}Fe_xBO_4$ has revealed the breakdown of the Mn^{2+}/Mn^{3+} charge ordering and the suppression of the long-range antiferromagnetic order in the latter. Fe-substitution induces the change in the crystal symmetry from monoclinic (sp. g. $P2_1/a$) for x = 0.0 to orthorhombic (sp.g. *Pnam*) for $x \geq 0.3$ and the reduction of local structural distortion around both Mn and Fe atoms. Here we report the Fe substitution effect on magnetism, including the magnetic anisotropy, and REHAC phase of the $Mn_{2-x}Fe_xBO_4$.

2. Experimental procedure

The crystal growth method and the structure of $Mn_{2-x}Fe_xBO_4$ (x = 0.3, 0.5, 0.7) warwickites were reported in a previous work [25]. Single crystalline samples of $Mn_{2-x}Fe_xBO_4$ were grown by the flux method in the system $Bi_2Mo_3O_{12}$–B_2O_3–Na_2O–Mn_2O_3–Fe_2O_3. Needle shape black crystals with a typical size of 0.4 × 0.2 × 8.0 mm^3 were obtained. The magnetic and heat-capacity measurements were performed using a Quantum Design PPMS (Physical Properties Measurement System). The temperature range was 2–300 K. The *dc* magnetization measurements were carried out for parallel (*c*-axis) and perpendicular (*ab*-plane) orientations of applied field respective the needle axis in magnetic fields up to 9 T. The *ac* magnetic susceptibility was measured in the frequency range $0.01 < f < 10$ kHz, with an exciting field of 5 Oe. Heat-capacity measurements as a function of temperature and magnetic field were performed employing 7.93, 8.44 and 6.49 mg of randomly oriented crystalline needles (x = 0.3, 0.5 and 0.7, respectively).

The high-temperature heat capacity were measured by DSC on a NETZSCH 204 F1 instrument in a dry helium flow (20 ml/min) in the 323–773 K temperature range at a heating rate of 5 K/min in aluminum specimen containers (V = 25 mm^3, d = 6 mm) equipped with lids with a hole. The average weight of the samples for heat capacity measurements was about 50 mg. Sapphire (m = 50.16 mg) was used as the standard. Three series of measurements were carried out for each crystal. The calibration against the heat flux was carried out before each measurement throughout the temperature range of interest. The experimental data were processed using the NETZSCH Proteus Thermal Analysis program package.

The Mössbauer absorption spectra of ^{57}Fe nuclei were recorded in the temperature range between 4 and 300 K with a standard MS-1104Em spectrometer operating in the constant accelerations regime. The gamma-ray source $^{57}Co(Cr)$ was at room temperature. The isomer shifts of Mössbauer spectra were measured relative to a metal α-Fe standard absorber. The hyperfine parameters were obtained by a least-square procedure assuming Lorentzian line shapes. A powder of crushed single crystals was used.

The morphology, microstructure and local elemental composition of the $Mn_{2-x}Fe_xBO_4$ (x = 0.3, 0.5, 0.7) samples were investigated using scanning and transmission electron microscopy (SEM and TEM). SEM experiments were performed with a JEOL JSM-7001F equipped with an energy dispersive X-ray spectrometer (Oxford Instruments) by which the elemental composition of the samples was controlled. TEM experiments were made with a JEOL JEM-2100 microscope operating at the accelerating voltage of 200 kV.

3. Experimental results and discussion

3.1. SEM, TEM and EDS characterization

Fig. 1a and b show the SEM images of the $Mn_{2-x}Fe_xBO_4$ samples demonstrating the shape of the single crystals which is characteristic for all the investigated samples.

In Fig. 2a the scanning transmission electron microscopy (STEM) image of the $Mn_{1.3}Fe_{0.7}BO_4$ sample is shown. Given in Table 2 is the normalized concentration of manganese and iron obtained from the points shown in Fig. 2a, which are good agreed with results of spectroscopic study and target stoichiometry [25]. Presented in Fig. 2b and c are the energy dispersive spectroscopy (EDS) elemental mapping images of Mn (b) and Fe (c) of the $Mn_{1.3}Fe_{0.7}BO_4$ sample. Based on the analysis of the elemental mapping images it is possible to conclude that manganese and iron are uniformly distributed throughout the sample, at least in the scale of 20–30 nm.

3.2. Mössbauer effect

The room-temperature Mössbauer spectra of $Mn_{2-x}Fe_xBO_4$ warwickites can be well described by four symmetric quadruple doublets D1-D4 (Fig. 3). The hyperfine parameters listed in Table 3 are comparable to those previously published [11,26]. The isomer shift values ($IS \approx 0.4$ mm/s) are close for all samples. A quadrupole splitting has a great difference ranged from QS = 0.5 to 1.60 mm/s, that is assigned to crystallographic nonequivalent metal sites M1 and M2 in the warwickite structure. As it was shown for $MgFeBO_4$ [8] and Mn_2BO_4 [19] the electrical field gradient V_{zz} of the M1 site is higher than the M2 site indicating pronounced distortions of $M1O_6$ oxygen octahedron. By analogy with previous ME data the doublets D3 and D4 with a greater QS value should be assign to the Fe^{3+} ions in the M1 site, while the doublets D1 and D2 are assigned to Fe^{3+} ions in the M2 site. The iron ions inter into the warwickite structure in the trivalent and high-spin states. As Fe

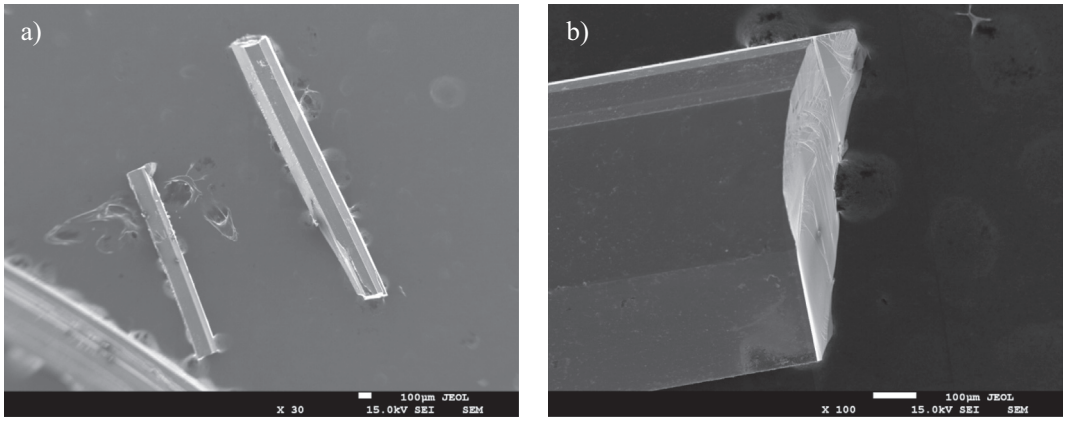

Fig. 1. SEM images of $Mn_{1.3}Fe_{0.7}BO_4$ (a) and $Mn_{1.5}Fe_{0.5}BO_4$ (b) samples.

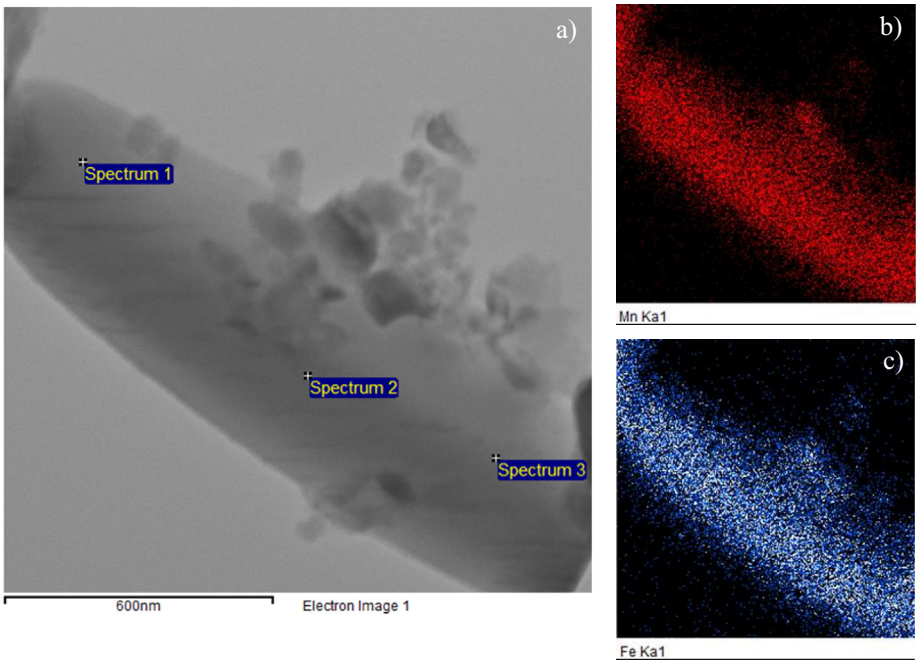

Fig. 2. STEM image (a) and corresponding EDS elemental mapping images of Mn (b) and Fe (c) of the $Mn_{1.3}Fe_{0.7}BO_4$ sample.

Table 2
The normalized concentration of manganese and iron of the $Mn_{1.3}Fe_{0.7}BO_4$ sample.

	Mn (at%)	Fe (at%)
Spectrum 1	64.5	35.5
Spectrum 2	63.5	36.5
Spectrum 3	63.7	36.3

content increase the distortions of both coordinated octahedra (*QS*) decrease agreeing with the results of the EXAFS study.

The occupation of the M1 and M2 sites by Fe^{3+} is independent on the concentration (~0.5/0.5) and indicates the uniform distribution of Fe^{3+} ions over two crystallographic positions. Based on the Mössbauer data, a cation distribution over M1 and M2 sites in $Mn_{2-x}Fe_xBO_4$ warwickites can be written as:

$$\begin{aligned} x = 0.3 &: (Mn_{0.84}Fe_{0.14})^{M1}(Mn_{0.86}Fe_{0.16})^{M2}BO_4 \\ x = 0.5 &: (Mn_{0.75}Fe_{0.25})^{M1}(Mn_{0.75}Fe_{0.25})^{M2}BO_4 \\ x = 0.7 &: (Mn_{0.65}Fe_{0.35})^{M1}(Mn_{0.65}Fe_{0.35})^{M2}BO_4 \end{aligned} \quad (1)$$

At same time each non-equivalent position represents by two quadrupole doublets with the area ratio ~2:1. That is, the distribution of iron over non-equivalent positions has signs a certain order within M1 and M2 positions.

As temperature decrease, the Mössbauer spectra split into sextets due to the Zeeman effect-indicating the magnetic ordering of iron ions (Fig. 4). A noticeable broadening of the outer lines of the spectrum is clearly observed, which indicates a heterogeneity of the Fe-cations magnetic surrounding in the crystal. In our study of $Mn_{1-x}Fe_xBO_4$ warwickites by Mössbauer spectroscopy we have used model hyperfine field distribution (HFD). The temperature evolution of the magnetic spectra is characterized by an increase of the hyperfine fields and a decrease of the width of HFD. The width of the HFD indicates the many possible magnetic states of the iron ions. The warwickites with cation disorder often display wide ranges of local environments leading to continuous distributions of hyperfine parameters. Fig. 5 shows the distribution of the hyperfine field probability in the experimental spectra, obtained at $T_1 \approx 0.6 \cdot T_{SG}$ and $T_2 \approx 0.4 \cdot T_{SG}$ for two Fe-rich samples ($x = 0.5$ and 0.7). These distributions are centered at ~400 for T_1 and 430 kOe

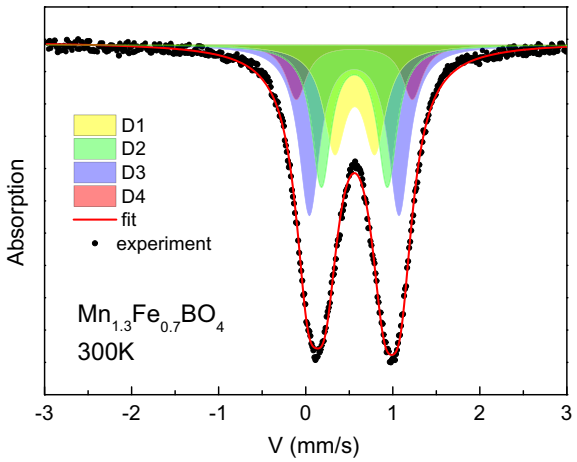

Fig. 3. Room-temperature Mössbauer spectrum of $Mn_{1.3}Fe_{0.7}BO_4$. The four quadrupole doublets D1-D4 corresponding to the M1 and M2 sites of Fe^{3+} ions are highlighted by the colors. (For interpretation of the references to color in this figure legend, the reader is referred to the web version of this article.)

for T_2. The blue solid lines correspond to the HFD averaged over ten points. It is clear, that HFD shows non-symmetric shape concerning to the maximums of the distribution. Asymmetry of the distribution increases with the temperature decrease.

Mössbauer spectra recorded at the temperature of 4 K are shown in Fig. 6. These spectra can be well approximated by two sextets with the hyperfine parameters listed in the Table 4. The average hyperfine magnetic field value (~450 kOe) is in fact somewhat higher than those known for other Fe-substituted warwickites [8,26]. The mentioned above a certain ordering of iron cations within the positions M1 and M2 observed at room temperature is exhibited in the occupations of the magnetic sextets at 4 K (~0.7/0.3) and the non-symmetric shape of the HFD at the temperatures below T_{SG}. The wide HFD demonstrates the existence in crystals of the regions ("clusters") with the different magnetic correlation radii. The random distribution of the "clusters" and random strength of the magnetic bond between them results in the spin-glass-like state in the Mn-Fe warwickites.

3.3. dc magnetization

Field cooled (FC) and zero field cooled (ZFC) *dc* magnetization measurements as a function of temperature with an applied field of 500 Oe parallel and perpendicular to *c*-axis are shown in

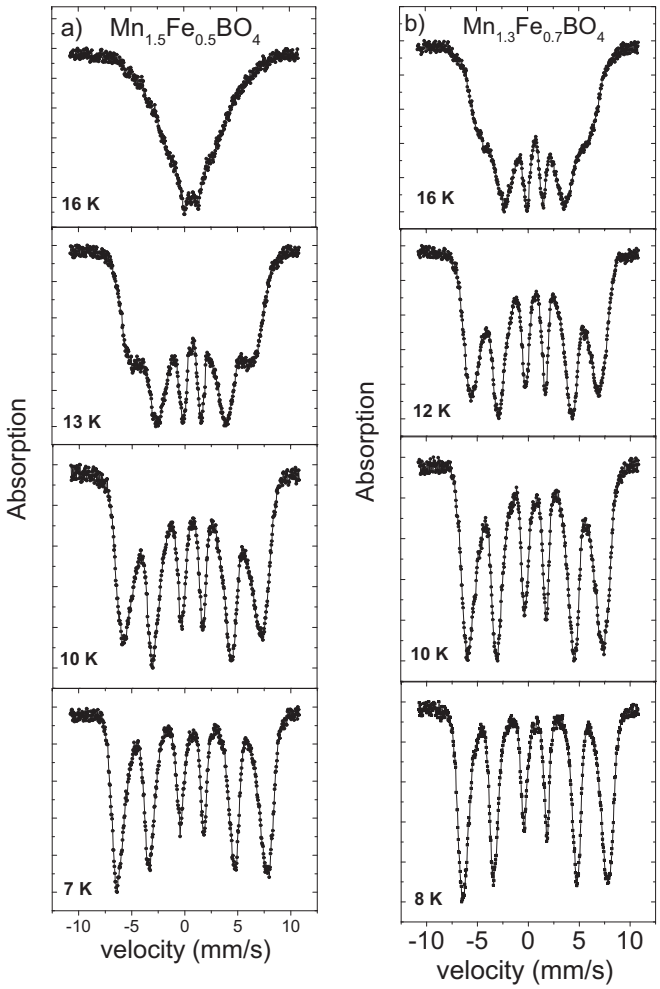

Fig. 4. Mössbauer spectra of a) $Mn_{1.5}Fe_{0.5}BO_4$ and b) $Mn_{1.3}Fe_{0.7}BO_4$ taken at temperatures below magnetic transition.

Fig. 7. A negligible anisotropy is found for all samples, while the mixed-valent Mn_2BO_4 displays an easy magnetization direction lying in the *ab*-plane [19]. It is to be expected since Mn^{3+}ions (d^4) are substituted by Fe^{3+} ions (d^5) having no orbital moment. Among other factors, the magnetocrystalline anisotropy depends on the actual distortion of first coordination shell. The Fe substitution induces the decrease in tetragonal distortions within both Fe

Table 3
Hyperfine parameters obtained from the RT Mössbauer spectra of $Mn_{2-x}Fe_xBO_4$ (x = 0.3, 0.5, 0.7). *IS* is the isomer shift relative to α-Fe (±0.01 mm/s), *QS* is the quadrupole splitting (±0.01 mm/s), *W* is the line width (±0.01 mm/s), and *A* is the iron occupation factor (±1.5%).

	IS (mm/s)	*QS* (mm/s)	*W* (mm/s)	*A* (%)	Fe site
$Mn_{1.7}Fe_{0.3}BO_4$					
D1	0.413	0.586	0.345	16	M2
D2	0.399	0.965	0.394	37	
D3	0.397	1.307	0.312	34	M1
D4	0.402	1.600	0.264	13	
$Mn_{1.5}Fe_{0.5}BO_4$					
D1	0.399	0.491	0.296	17	M2
D2	0.401	0.799	0.327	33	
D3	0.399	1.113	0.346	36	M1
D4	0.397	1.435	0.332	14	
$Mn_{1.3}Fe_{0.7}BO_4$					
D1	0.404	0.443	0.283	16	M2
D2	0.398	0.752	0.320	34	
D3	0.351	1.068	0.327	33	M1
D4	0.476	1.072	0.300	17	

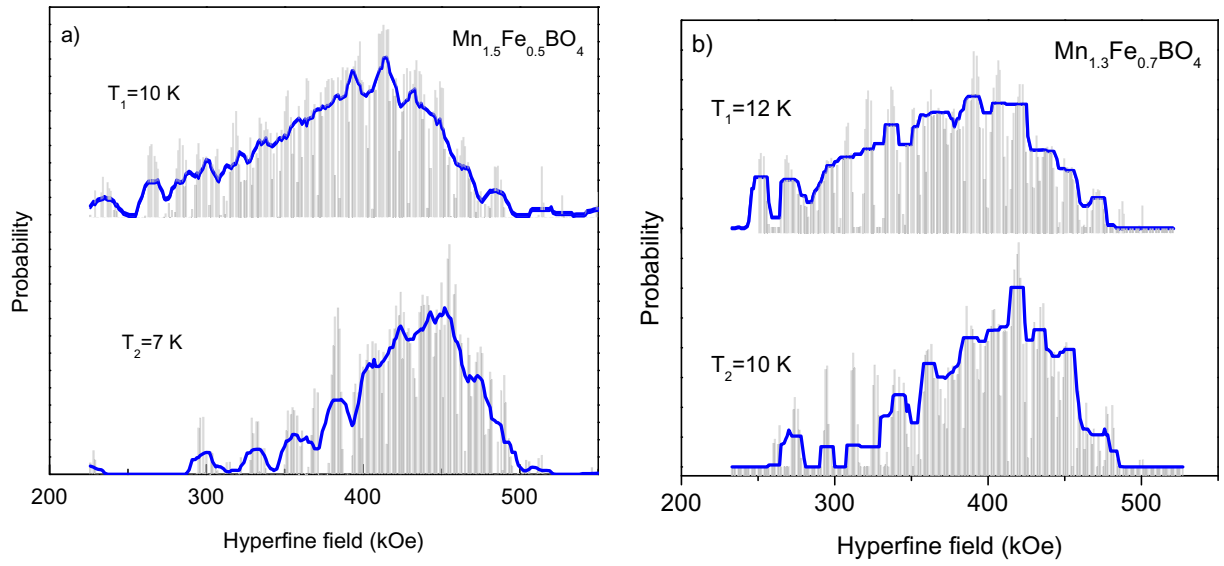

Fig. 5. Hyperfine field distributions for a) $Mn_{1.5}Fe_{0.5}BO_4$ and b) $Mn_{1.3}Fe_{0.7}BO_4$ as obtained from experimental Mössbauer spectra and averaging over ten points (blue line). (For interpretation of the references to color in this figure legend, the reader is referred to the web version of this article.)

and Mn types of coordinated octahedra and thereby reducing the magnetic anisotropy [25]. The inset to Fig. 7b presents the comparison of the FC magnetization versus temperature curves of Mn-based warwickites at the applied field of 50 kOe parallel to *c*-axis. The introduction of the Fe gives raises the significant increase in the magnetic moment.

All three samples demonstrates a peak on the ZFC curves and a strong thermo-irreversibility between the ZFC and the FC data, a behavior found to be typical of a spin-glass (SG) state. For the lower temperatures the ZFC curve falls off rapidly while the FC curve monotonically increases up to the lowest temperatures. The temperature of the maximum (T_m) as well as the temperature (T_{irr}) where the irreversibility between the ZFC and FC curves appears depend on the applied magnetic field (inset to Fig. 7a). As applied field increase the ZFC cusp broadens and is shifted to lower temperature. The temperature T_m is increase steadily with Fe content: ~11, 14 and 17 K for $x = 0.3$, 0.5 and 0.7, respectively (Table 5). At sufficiently high temperatures ($T > 220$ K) the *dc* magnetic susceptibility ($\chi_{dc} = M/H$) is described by the Curie–Weiss law (inset to Fig. 7c). As temperature decrease the susceptibility exhibits progressive deviation from Curie-Weiss behavior indicating the growing short-range-order (SRO) spin correlations. A characteristic temperature T_d at which the deviations appear is as large as one order of magnitude the T_{SG} (Table 5). This suggests that the SRO spin correlations develop long before the spin-glass transition. In $Mn_{2-x}Fe_xBO_4$ warwickites the effective magnetic moments of μ_{eff}^{exp} for two directions of applied field are close to each other (the difference is about 5%). Furthermore, the respective temperatures θ and T_d for the fields applied along *ab*-plane differ at most by 5% from those for the field parallel to the *c*-axis confirming the reducing of the magnetic anisotropy. The values obtained from the Curie-Weiss fit for the applied field parallel to *c*-axis are listed in Table 5. The enhancement of afm interactions manifests in the increasing of negative Curie-Weiss temperature θ with Fe content. A simple experimental measure of the exchange energy is provided by the constant θ, which according to mean field theory is given by $\theta = \frac{2S(S+1)}{3k_B}\sum_i^z J_i$, where z_i is the number of nearest-neighbors with exchange coupling J_i. We used $z = 2$ and the average spin per ion (for substituted $Mn_{2-x}Fe_xBO_4$ system the formula unit involves one Mn^{2+} ion and mixture of Mn^{3+} and Fe^{3+} ions taken with the weights of $(1-x)$ and x, respectively). The estimated exchange parameters J/k_B increases from ~12 to ~1 K for $x = 0.0$ and 0.7, respectively

(Table 5), i.e. the energy scale for the antiferromagnetic interactions increases. We estimated the expected values of the effective magnetic moments considering that the orbital component of magnetic moment is neglected. Assuming the high-spin states for all ions $S(Mn^{2+}) = S(Fe^{3+}) = S1 = 5/2$, $S(Mn^{3+}) = S2 = 2$ and $g = 2$ the spin component of the effective moment calculated according with the formula [27]

$$\mu_{eff}^{S} = g \cdot \sqrt{(1+x)\cdot S1\cdot(S1+1) + (1-x)\cdot S2\cdot(S2+1)}. \quad (2)$$

are given in Table 5. For all studied samples the deviation of μ_{eff}^{exp} from the expected effective moment μ_{eff}^{S} is observed. In addition, the μ_{eff}^{exp} demonstrate the monotonic decrease with *x*, that strongly contrasts with the expected increasing of the μ_{eff}^{S}. At the high temperatures where disordering temperature effect is large, the effective moment is to be close to the free-ion effective moment. In spin-glass systems the afm SRO spin correlations induce the deviation from the paramagnetic behavior and are evident in the temperature variation of μ_{eff}^{exp} [28]

$$\mu_{eff}^{exp}(T) = (3k_B)^{1/2}\left(\frac{d(\chi_{dc}^{-1})}{dT}\right)^{-1/2}, \quad (3)$$

k_B is a Boltzmann constant. The effective magnetic moments derived in this way are shown in the inset to Fig. 8. The effective moment μ_{eff}^{exp} of Mn_2BO_4 is constant above T_d and gradually decreases below T_d while the substituted samples show monotonic decrease over *T* range. This indicates that at the finite temperatures $T > T_{SG}$ the part of the spin system is remain interacting. The number of the non-interacting (paramagnetic) spins N_{eff}^{PM} can be extracted from the *dc* susceptibility data as has been demonstrated in Ref. [29]. For spin-glass system with predominantly afm interactions an enhancement of $\chi^{exp}(T)$ above the extrapolated high-temperature Curie-Weiss behavior $\chi(T) = \frac{C_0}{T-\theta}$ and the depression below a fictive Curie law $\chi^0(T) = \frac{C_0}{T}$, $C_0 = \frac{Ng^2\mu_B^2 S(S+1)}{3k_B}$, where *N* is the total number of spins in the system, are expected. The magnetic susceptibility depending on the temperature and effective number N_{eff}^{PM} may be obtained in the Curie form $\chi(T) = \frac{C_0}{T}N_{eff}^{PM}(T)$. The derived

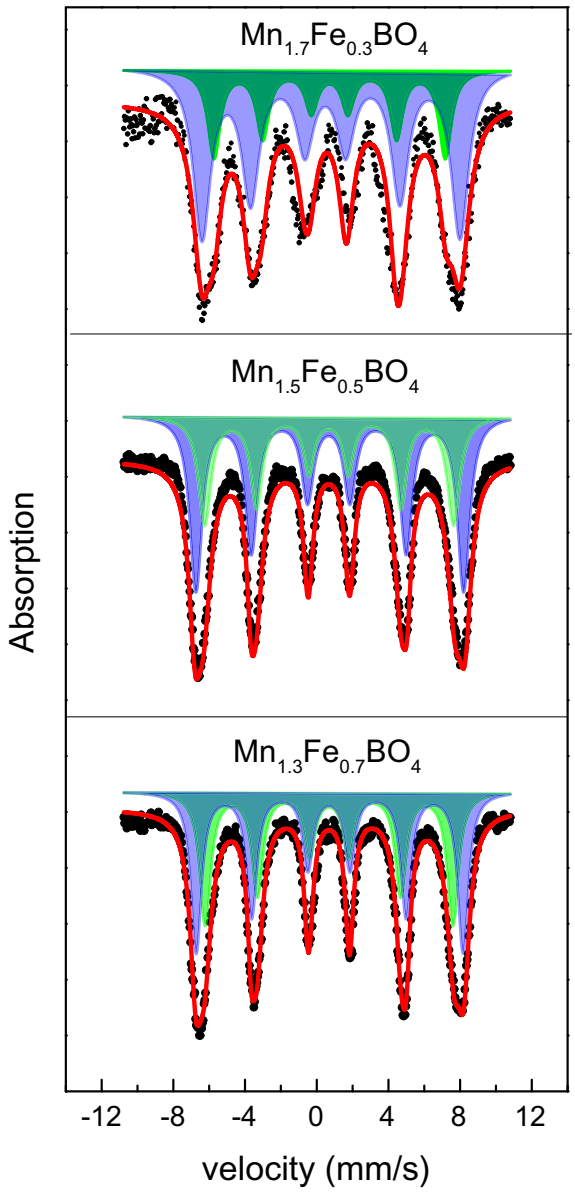

Fig. 6. Low temperature Mössbauer spectra of $Mn_{1-x}Fe_xBO_4$. The calculated spectrum components with hyperfine parameters listed in Table 4 are highlighted by the colors. (For interpretation of the references to color in this figure legend, the reader is referred to the web version of this article.)

values of $N_{eff}^{PM}(T)$ are shown in Fig. 8. As temperature decreases the $N_{eff}^{PM}(T)$ behavior demonstrates monotonically decrease related with growing SRO spin correlations. Below T_{SG} the $N_{eff}^{PM}(T)$ rapidly tends to zero indicating that all spins are became magnetically coupled. We have estimated the effective number of the interacting spins N_{eff}^{int} which is linked with the number of the paramagnetic spins N_{eff}^{PM} by simple relation $N_{eff}^{int} = 1 - N_{eff}^{PM}$. The room temperature value of interacting spin concentration $N_{eff}^{int} \approx 0.49$, 0.52, and 0.61 for x = 0.3, 0.5, and 0.7, respectively, that is sufficiently larger than that for pure paramagnetic state.

For all samples the field dependences of the magnetization at lowest measured temperature exhibit a rounded shape without any trend to saturation up to 9 T (Fig. 9). The magnetization value at 9 T reaches a small fraction of the calculated saturation. Hysteresis loops are observed at low temperatures, which is a signature of the spin-glass state. This behavior is strongly contrasts with the linear dependence expected for LRO antiferromagnetism actually observed for Mn_2BO_4 [19].

3.4. ac magnetic susceptibility

The other feature supporting the indication of a SG ground state in Fe-substituted samples is the *ac* magnetic susceptibility. All samples show relatively sharp maxima of real component of magnetic susceptibility χ' and a step-like behavior of imaginary part of susceptibility χ'' at the freezing temperature T_f. The temperature behavior of $\chi'(T)$ for different frequencies of the driving *ac* field (f) is shown in Fig. 10 for $Mn_{1.3}Fe_{0.7}BO_4$ as an example. For lower frequencies the observed maxima of $\chi'(T)$ are shifted to lower temperatures and the absolute values of $\chi'(T)$ are increased (top inset Fig. 10). The increase of the maximum intensity is about a 5% of the peak value. The freezing temperatures T_f are frequency dependent. The normalized frequency shift defined as $p = \Delta T_f/T_f \cdot (\Delta \log f)$ is equal 0.028, 0.023 and 0.030 for x = 0.3, 0.5 and 0.7, respectively. These values match well with those found in Mg-Co-Fe warwickites [8]. In order to analyze the maximum frequency dependence, we have scaled our data using a critical law $f = f_0(T_f(f)/T_f(0) - 1)^{z\nu}$ where $T_f(f)$ is the spin-glass transition temperature as a function of the frequency, $T_f(0)$ is the spin-glass transition temperature in the limit of zero frequency, $z\nu$ is the dynamic critical exponent. The results are shown in the bottom inset to Fig. 10. The best fit parameters are given in Table 6. Evidently, the characteristic parameter f_0 is larger than the value for canonical spin glass system (10^{10}–10^{13} Hz) [30,31] and decreases with increasing of Fe content. The dynamic critical exponent $3.95 \leq z\nu \leq 5.51$ are close to that found for cluster spin-glasses such as hole-doped manganites [32].

The field dependence of the freezing temperature follows a potential law $H(T) = H(0)\cdot[1 - T_f(H)/T_f(0)]^{\gamma}$ (Fig. 11). The linear fit yields $T_f(0)$ = 17.6 K, $H(0)$ = 95.5(2) kOe, γ = 1.07(2) for $Mn_{1.3}Fe_{0.7}BO_4$. Note that the parameter γ is lower than that for Almeida-Thouless irreversibility line (~1.50).

Taking into account the quasi low-dimensional character of the magnetic interactions in the warwickites one can expected that above T_{SG} the afm short-range spin correlations will lead to the formation of one-dimensional Heisenberg spin chains. Evidence for a quasi 1D magnetic behavior in the warwickites has been obtained earlier [7,8,12–14] and comes from the intermediate-temperature

Table 4
Mössbauer parameters of $Mn_{2-x}Fe_xBO_4$ (x = 0.3, 0.5, 0.7) obtained at T = 4 K. *IS* is the isomer shift relative to α-Fe (±0.01 mm/s), H_{hf} is the magnetic hyperfine field at Fe nuclei (±5 kOe), *QS* is the quadruple splitting (±0.02 mm/s), *W* is the half-line width (±0.06 mm/s), and *A* is the iron occupation factor (±1.5%).

		IS (mm/s)	H_{hf} (kOe)	*QS* (mm/s)	*W* (mm/s)	*A* (%)
$Mn_{1.7}Fe_{0.3}BO_4$	S1	0.494	449	0.61	1.04	0.68
	S2	0.550	403	0.16	0.86	0.32
$Mn_{1.5}Fe_{0.5}BO_4$	S1	0.550	464	0.12	0.74	0.68
	S2	0.532	431	0.01	0.72	0.32
$Mn_{1.3}Fe_{0.7}BO_4$	S1	0.549	463	0.09	0.64	0.53
	S2	0.540	431	0.01	0.69	0.48

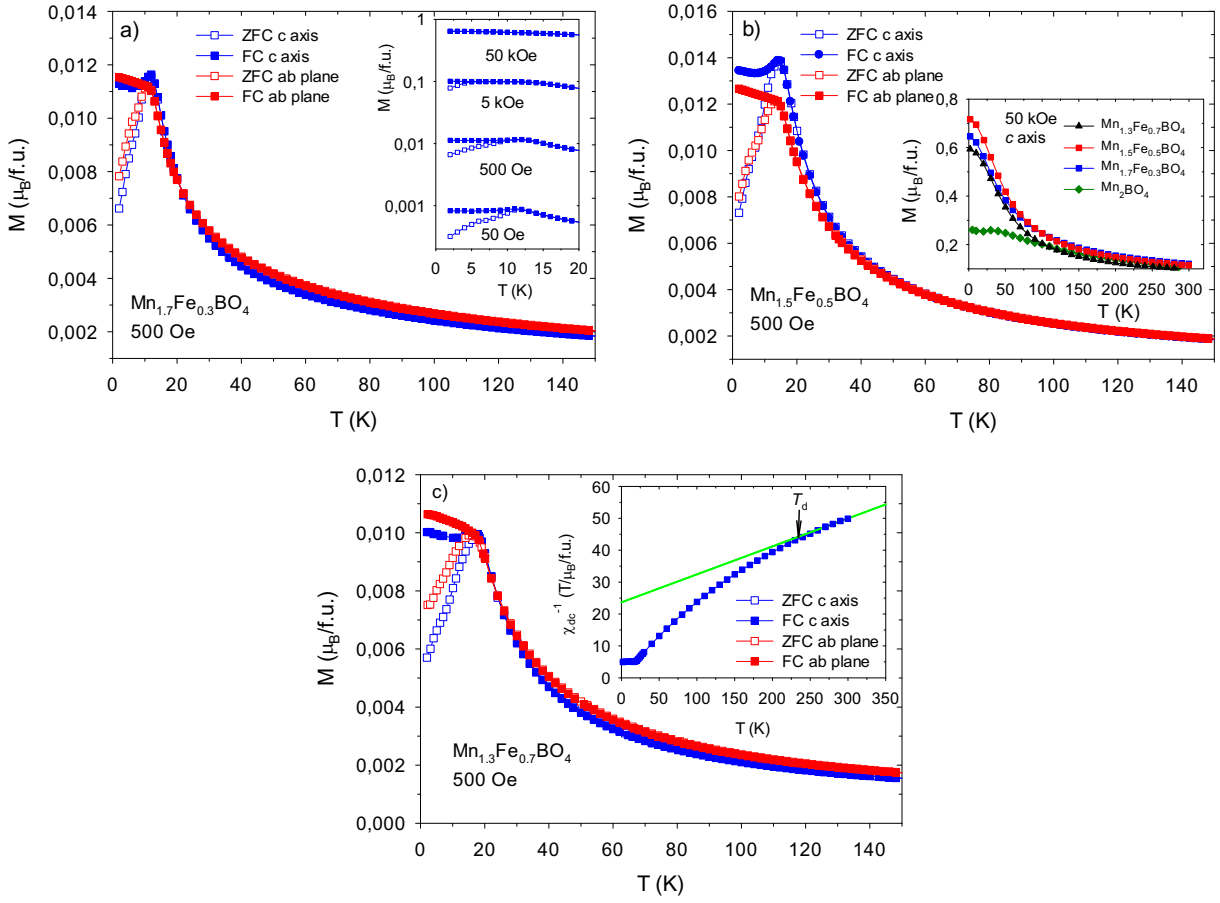

Fig. 7. Temperature dependences of the ZFC and FC magnetizations at H = 500 Oe, showing the SG behavior for a) $Mn_{1.7}Fe_{0.3}BO_4$, b) $Mn_{1.5}Fe_{0.5}BO_4$, c) $Mn_{1.3}Fe_{0.7}BO_4$. The insets: a) the field-dependent splitting of ZFC and FC curves at the external magnetic field parallel to *c*-axis; b) temperature dependences of the FC magnetizations of Mn_2BO_4 and $Mn_{2-x}Fe_xBO_4$ (x = 0.3, 0.5, 0.7) at field of 50 kOe parallel *c*-axis; c) inverse *dc* susceptibility as a function of the temperature for $Mn_{1.3}Fe_{0.7}BO_4$. The temperature T_d denotes the onset of the deviations from Curie-Weiss behavior.

Table 5
Magnetic parameters of $Mn_{2-x}Fe_xBO_4$ (x = 0.3, 0.5, 0.7) obtained from *dc* magnetization data (H = 500 Oe). The parameters for Mn_2BO_4 are taken from the Ref. [19]. The applied field is parallel to *c*-axis.

	Mn_2BO_4	$Mn_{1.7}Fe_{0.3}BO_4$	$Mn_{1.5}Fe_{0.5}BO_4$	$Mn_{1.3}Fe_{0.7}BO_4$
T_N, T_m, K	26	11.3	14.6	16.9
T_d, K	100	220	220	236
μ_{eff}^{exp}, μ_B/f.u.	6.25	7.08	7.01	6.87
θ, K	−118	−177	−171	−228
$\lvert\theta/T_m\rvert$	4.5	15.7	11.7	13.5
J/k_B, K	12.1	17.2	16.3	20.6
μ_{eff}^{c}, μ_B/f.u.	7.68	7.92	8.01	8.18

ac susceptibility where the power law of $\chi(T) = A \cdot T^{-\alpha}$ is obeyed (characteristic of Random Exchange Heisenberg Antiferromagnetic Chain, REHAC [33,34]). Indeed, we have observed such power law behavior in all samples in the double log plot of $\chi(T)$ (inset to Fig. 12). The fitting parameters are listed in Table 7. The fitted temperature range was from ~33 to 196 K. The exponent α is ranged from 0.76 to 0.88 depending on the iron concentration and close to that found in other warwickites [7,8]. The renormalization calculations have shown that the power-law with $\alpha \sim 0.8$ is a quasi-universal behavior for a wide class of distributions of exchange parameters J [33]. The deviation from the $T^{-\alpha}$ behavior has been observed as the temperature approached the T_{SG} where the exponent increases up to ~0.9–0.93. The satisfactory fit of the experimental $\chi_{ac}(T)$ by power law is shown in Fig. 12 for $Mn_{1.3}Fe_{0.7}BO_4$. Thus, the intermediate temperature interval, between the spin-glass transition and paramagnetic behavior, is characterized by the formation of localized spins chains with random antiferromagnetic interactions.

3.5. Heat capacity

The results of the heat capacity (HC) measurements are shown in Fig. 13 where the comparison with the data for mixed-valent Mn_2BO_4 is represented. The Fe-containing warwickites display broad anomalies with the maximum around ~11, 15, and 18 K for x = 0.3, 0.5 and 0.7, respectively, associated with spin-glass transitions, while the heat capacity of Mn_2BO_4 shows a sharp λ-type anomaly at 23 K due to long-range magnetic ordering. As Fe content increase the maximum becomes smeared out and is decreased in intensity. The magnetic field up to 9 T has weak effect

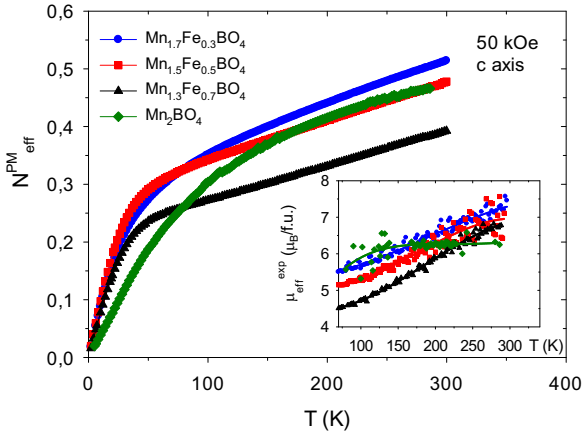

Fig. 8. Temperature dependence of the effective number of non-interacting magnetic moments. The inset shows the thermal variance of effective magnetic moment defined following Eq. (3).

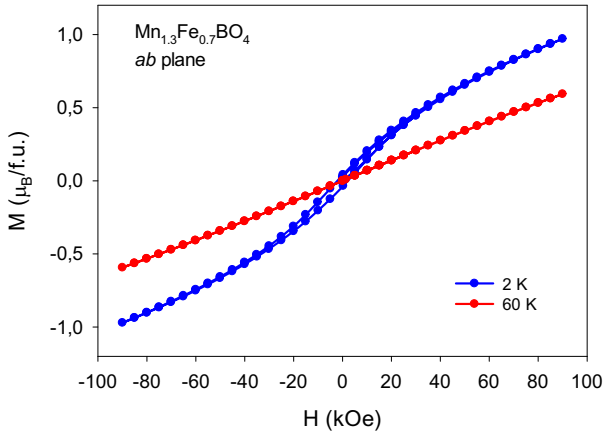

Fig. 9. Field dependences of the magnetization for $Mn_{1.3}Fe_{0.7}BO_4$ single crystal at 2 and 60 K for field perpendicular to needle axis.

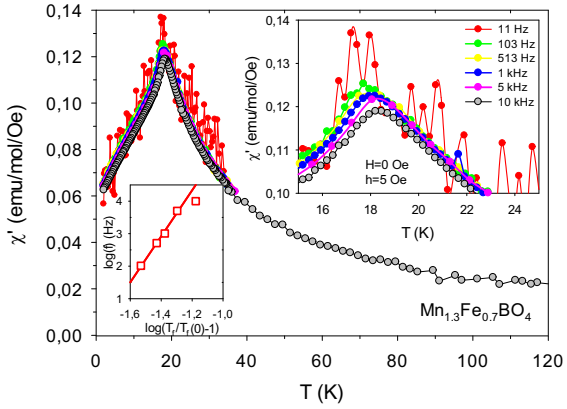

Fig. 10. Temperature dependence of the real part of *ac* susceptibility for $Mn_{1.3}Fe_{0.7}BO_4$ for different frequencies of the driving *ac* field when H = 0 Oe and *h* = 5 Oe. Top inset: the maximum frequency dependence. Bottom inset: the frequency dependencies of the spin-glass temperature plotted in the double log plot. The solid line is the fit to a critical-slowing-down model.

on the heat capacity of all Fe-containing samples (bottom inset to Fig. 13). In magnetic field the anomaly slightly smears out and shifts to lower temperatures. The HC of $Mn_{2-x}Fe_xBO_4$ warwickites does not follow a T^3 law even at the lowest temperatures. The lattice phonon contribution in the Debye-Einstein approximation

Table 6
Fit parameters for the χ_{ac} maximum frequency dependence.

	$Mn_{1.7}Fe_{0.3}BO_4$	$Mn_{1.5}Fe_{0.5}BO_4$	$Mn_{1.3}Fe_{0.7}BO_4$
f_0, Hz	$(8.11 \pm 0.28)\cdot 10^9$	$(2.84 \pm 0.95)\cdot 10^9$	$(0.14 \pm 0.02)\cdot 10^9$
zv	5.51 ± 0.14	4.66 ± 0.12	3.95 ± 0.07
T_{SG}, K	11.5 ± 0.2	14.4 ± 0.2	17.2 ± 0.2

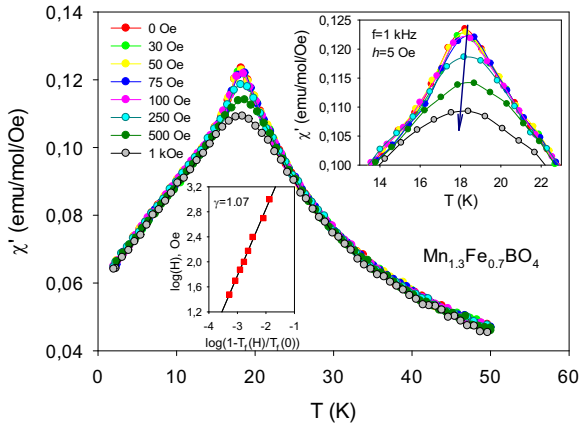

Fig. 11. Temperature dependence of the real part of *ac* susceptibility for $Mn_{1.3}Fe_{0.7}BO_4$ in the presence of a static magnetic field H, *h* = 5 Oe, *f* = 1 kHz. Top inset: field dependence of the maximum on a large scale. Bottom inset: the dependence of the freezing temperature on the static field.

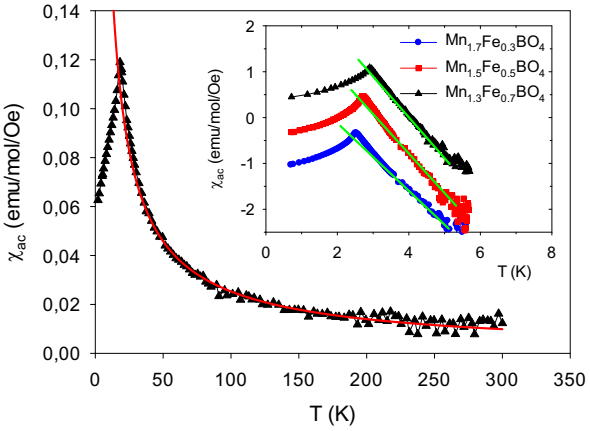

Fig. 12. *ac* magnetic susceptibility for $Mn_{1.3}Fe_{0.7}BO_4$ (*w* = 10 kHz) as a function of the temperature. Solid red line represents a fit of the power law $\chi(T) = A{\cdot}T^{-\alpha}$ with fitting parameters A = 1.87 and $\alpha = 0.85$. Inset shows the of $\chi(T)$ curves in double logarithmic scale. The straight lines denote the power law. Results for samples *x* = 0.5 and 0.7 are shifted upward for clarity. (For interpretation of the references to color in this figure legend, the reader is referred to the web version of this article.)

Table 7
Best fit parameters for the χ_{ac} temperature dependence.

	$Mn_{1.7}Fe_{0.3}BO_4$	$Mn_{1.5}Fe_{0.5}BO_4$	$Mn_{1.3}Fe_{0.7}BO_4$
A, emu/mol/Oe	1.46 ± 0.05	2.06 ± 0.08	1.87 ± 0.06
α	0.76 ± 0.01	0.88 ± 0.02	0.85 ± 0.01

$C^{latt}/R = K_D D(\Theta_D/T) + K_E D(\Theta_E/T)$ has been removed according to the procedure described in Ref. [19] for Mn_2BO_4. For fitting procedure the temperatures of $T > 120$ K and $T < 3.5$ K far from anomalous regions were used (top inset to Fig. 13). The parameters Θ_D and Θ_E depend on the fit *T* range displaying monotonic decrease with Fe content (Table 8). Note, that the obtained values of Θ_D and Θ_E for Mn_2BO_4 are larger than those previously reported

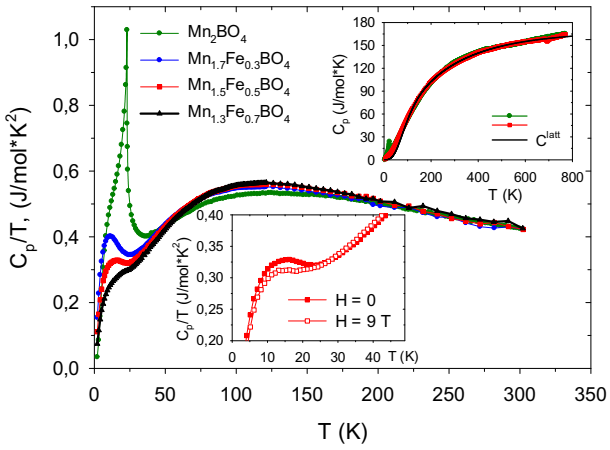

Fig. 13. Heat capacity of $Mn_{2-x}Fe_xBO_4$ (x = 0.0, 0.3, 0.5, 0.7) plotted as C/T vs T, H = 0. Top inset: experimental HC of Mn_2BO_4 and $Mn_{1.5}Fe_{0.5}BO_4$ and the lattice contribution to the HC of the latter (black solid line), H = 0. Bottom inset: $Mn_{1.5}Fe_{0.5}BO_4$ heat capacity for applied fields 0 and 9 T.

Table 8
The parameters obtained from fits of Debye-Einstein model to the high-temperature heat capacity of $Mn_{2-x}Fe_xBO_4$.

	Mn_2BO_4	$Mn_{1.7}Fe_{0.3}BO_4$	$Mn_{1.5}Fe_{0.5}BO_4$	$Mn_{1.3}Fe_{0.7}BO_4$
Θ_D, K	512	449	441	408
Θ_E, K	1399	1283	1140	1015
ΔS^{exp}, J/mol·K	26.8	18.2	15.5	11.8
ΔS^{th}, J/mol·K	28.3	28.7	29.1	29.3

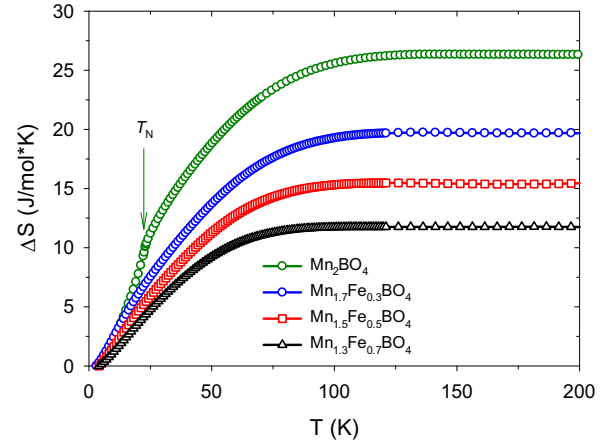

Fig. 14. Entropy as a function of temperature for $Mn_{2-x}Fe_xBO_4$ (x = 0.0, 0.3, 0.5, 0.7), H = 0. The antiferromagnetic transition in Mn_2BO_4 is shown by an arrow.

[19]. The reduction of lattice stiffness related to decrease of Jahn-Teller distortions is expected and is in accordance with EXAFS data [25]. The magnetic entropy ΔS^{exp} lies between ~26.3 and 11.8 J/mol·K (Fig. 14, and the third row in Table 8). These entropy values are much smaller than those estimated within the mean-field model with the number of magnetically active ions per formula unit n = 2 and the gas constant R = 8.314 J/mol K. For the system containing two types of the spins S1 and S2 as denoted in *Sec. 3.3* $\Delta S^{th} = R[(1+x)\cdot ln(2\cdot S1+1) + (1-x)\cdot ln(2\cdot S2+1)]$ (the fourth row in Table 8). The possible explanation for this "missing" entropy is that a considerable amount of entropy is given up at temperatures much higher than T_{SG}, due to the presence of short-range correlations. We may therefore expect a reduction in the change in entropy associated with this magnetic contribution.

4. Conclusion

The dynamic and static magnetic properties as well as Mossbauer effect and heat capacity have been investigated in $Mn_{2-x}Fe_xBO_4$ with x = 0.3, 0.5, 0.7. A clear transition to a SG-like state is identified by a sharp maximum $\chi_{ac}(T)$ at the freezing temperature T_f, accompanied by onset of a dependence of χ_{ac} on the f. The frequency dependence of the $T_f(f)$ is well described with the conventional critical slowing-down law with the glass temperature increasing with the Fe content increasing. Due to the Fe^{3+} (S = 5/2) substitution for Mn^{3+} (S = 2) and unit cell decrease the enhancement of the average magnetic exchange interactions is expected, an effect which is perceptible through the increase in magnetic transition temperature (T_{SG}). The iron introduction reduces the magnetic anisotropy. The Mössbauer spectroscopy has revealed the feature of the cation distribution. While the iron ions occupy different crystallographic sites M1 and M2 without any brightly pronounced preference, the cation distribution within the sites was found to have a certain order. Each of the positions is divided into two ones with the occupation factors of Fe^{3+} equal 2:1. The non-symmetric shape of the HFD's below spin-glass transition temperature and the relaxation effects important at approaching T_{sg} have been found. The origins of spin-glass state in Mn-Fe warwickite can be due to random coupling between spatially separated spin-correlated regions ("clusters"). The Fe addition results in the increasing of AFM spin order within the "clusters" that is reflected in the deviations from Curie-Weiss law, the reduced effective magnetic moment and "missing" entropy. In addition, formation of "clusters" is also supported by the large relaxation times from a critical-slowing-down law ($\tau_0 = 1/f_0 = 10^{-9}$–10^{-8} s). The EDS mapping shows uniform distribution of Mn and Fe throughout the sample in the scale of 20–30 nm. This is indicates that the "clusters" have indeed the magnetic origin but not chemical. As Fe concentration increase the role of SRO spin correlations increase, that results in the increase of the number of magnetically coupling spins at definite temperatures ($T > T_{SG}$). The random coupling between spin-correlated regions is due to the competitive exchange interactions leading to dramatic increase in frustration index from $f \sim 5$ for Mn_2BO_4 to ~13.5 in $Mn_{2-x}Fe_xBO_4$ and tip the balance from LRO towards a spin-glass state. In the presence of Fe ions we always expect the enhancement of SRO spin correlation independently on the kinds of M^{2+} ion (Table 1). Nevertheless, the temperature T_d when these correlations become effective was found maximal for Mn-Fe warwickites than for the other reported heterometallic warwickites. The three compounds show REHAC behavior $\chi(T) = A\cdot T^{-\alpha}$ in the intermediate temperature range that is the general peculiarity of the warwickite structure. The α parameters have been deduced as a function of temperature and Fe.

Acknowledgments

This study was supported in part by the grants of: The Council for Grants of the President of the Russian Federation (project nos. SP-938.2015.5, NSh-7559.2016.2), the Russian Foundation for Basic Research (project nos. 16-32-60049 mol_a_dk, 16-32-00206 mol_a, 17-02-00826-a, 16-32-50058). The magnetic measurements were carried out in the Shared Facility Centre of P. N. Lebedev Physical Institute of RAS.

References

[1] L. Balents, Spin liquids in frustrated magnets, Nature 464 (2010) 199–208.
[2] N.J. Laurita, J. Deisenhofer, LiDong Pan, C.M. Morris, M. Schmidt, M. Johnsson, V. Tsurkan, A. Loidl, N.P. Armitage, Singlet-triplet excitations and long-range entanglement in the spin-orbital liquid candidate $FeSc_2S_4$, Phys. Rev. Lett. 114 (2015) 207201.

[3] A.P. Ramirez, Strongly geometrically frustrated magnets, Ann. Rev. Mater. Sci. 24 (1) (1994) 453–480.
[4] J.E. Greedan, Geometrically frustrated magnetic materials, J. Mater. Chem. 11 (2001) 37–53.
[5] M. Taillefumier, J. Robert, C.L. Henley, R. Moessner, B. Canals, Semiclassical spin dynamics of the antiferromagnetic Heisenberg model on the kagome lattice, Phys. Rev. B 90 (6) (2014) 064419.
[6] A.P. Ramirez, A. Hayashi, R.J. Cava, R. Siddharthan, B.S. Shastry, Zero-point entropy in 'spin ice', Nature 399 (1999) 333–335.
[7] R.B. Guimaraes, J.C. Fernandes, M.A. Continentino, H.A. Borges, C.S. Moura, J.B. M. Da Cunha, C.A. Dos Santos, Dimensional crossover in magnetic warwickites, Phys. Rev. B 56 (1) (1997) 292–299.
[8] A. Arauzo, N.V. Kazak, N.B. Ivanova, M.S. Platunov, Yu.V. Knyazev, O.A. Bayukov, L.N. Bezmaternykh, I.S. Lyubutin, K.V. Frolov, S.G. Ovchinnikov, J. Bartolomé, Spin-glass behavior in single crystals of hetero-metallic magnetic warwickites $MgFeBO_4$, $Mg_{0.5}Co_{0.5}FeBO_4$, and $CoFeBO_4$, J. Magn. Magn. Mater. 392 (2015) 114–125.
[9] D.C. Freitas, C.P.C. Medrano, D.R. Sanchez, M.N. Regueiro, J.A. Rodríguez-Velamazán, M.A. Continentino, Magnetism and charge order in the ladder compound $Co_3O_2BO_3$, Phys. Rev. B 94 (17) (2016) 174409, and references therein.
[10] Yu.V. Knyazev, N.V. Kazak, I.I. Nazarenko, S.N. Sofronova, M.S. Platunov, S.G. Ovchinnikov, Crucial Role of Frustrations in Magnetic Ground-state of Fe3BO5 Ludwigite, prepared for publication (2017).
[11] I.S. Lyubutin, N.Yu. Korotkov, K.V. Frolov, N.V. Kazak, M.S. Platunov, Yu.V. Knyazev, L.N. Bezmaternyh, S.G. Ovchinnikov, A. Arauzo, J. Bartolomé, Spin-glass behavior of warwickite $MgFeBO_4$ and $CoFeBO_4$ crystals observed by Mossbauer spectroscopy, J. Alloy Compd. 642 (2015) 204–209.
[12] J.C. Fernandes, R.B. Guimaraes, M.A. Continentino, H.A. Borges, J.V. Valarelli, A. Lacerda, Titanium-III warwickites: a family of one-dimensional disordered magnetic systems, Phys. Rev. B 50 (1994) 16754–16757.
[13] M. Brunner, J.L. Tholence, L. Puech, S. Haan, J.J. Capponi, R. Calemczuk, J.C. Fernandes, M.A. Continentino, Low-energy excitations in the random magnetic chain system $MgTiBO_4$, Phys. Rev. B 233 (1997) 37–42.
[14] T.G. Rappoport, L. Ghivelder, J.C. Fernandes, R.B. Guimarães, M.A. Continentino, Experimental observation of quantum entanglement in low-dimensional spin systems, Phys. Rev. B 75 (2007) 054422.
[15] B. Rivas-Murias, F. Rivadulla, M. Sanchez-Andujar, A. Castro-Couceiro, M.A. Senarıs-Rodrıguez, J. Rivas, Role of t_{2g} versus e_g interactions in the physical properties of A_2OBO_3 (A = Mn, Fe), Chem. Mater. 18 (2006) 4547–4552.
[16] M.A. Continentino, A.M. Pedreira, R.B. Guimaraes, M. Mir, J.C. Fernandes, R.S. Freitas, L. Ghivelder, Specific heat and magnetization studies of Fe_2OBO_3, Mn_2OBO_3, and $MgScOBO_3$, Phys. Rev. B 64 (1) (2001) 014406.
[17] R. Norrestam, M. Kritikos, A. Sjodin, Manganese (II, III) Oxyborate, Mn_2OBO_3: a distorted homometallic warwickite-synthesis, crystal structure, band calculations, and magnetic susceptibility, J. Solid State Chem. 114 (1995) 311–316.
[18] R.J. Goff, A.J. Williams, J.P. Attfield, Spin, charge, and orbital order in Mn_2OBO_3, Phys. Rev. B 70 (2004) 0144261–0144265.
[19] N.V. Kazak, M.S. Platunov, Yu.V. Knyazev, N.B. Ivanova, O.A. Bayukov, A.D. Vasiliev, L.N. Bezmaternykh, V.I. Nizhankovskii, S.Yu. Gavrilkin, K.V. Lamonova, S.G. Ovchinnikov, Uniaxial anisotropy and low-temperature antiferromagnetism of Mn_2BO_4 single crystal, J. Magn. Magn. Mater. 393 (2015) 316–324.
[20] Q.A. Pankhurst, M.F. Thomas, B.M. Wanklyn, The electric field gradient in the quasi-one-dimensional disordered compound $FeMgBO_4$, J. Phys. C: Solid State Phys. 18 (6) (1985) 1255.
[21] A. Wiedenmann, F. Mezei, Edwards-Anderson type relaxation in the frustraded quasi-1d spin glass $FeMgBO_4$, J. Magn. Magn. Mater. 54 (1986) 103–104, and references therein.
[22] A. Apostolov, M. Mikhov, P. Tcholakov, Magnetic properties of boron ferrites $FeBMeO_4$, Phys. Status Solidi A 56 (1979) K33–K36.
[23] J.J. Capponi, J. Chenavas, J.C. Joubert, Sur de Nouveaux Borates Mixtes des Metaux de Transition Isotypes de la Warwickite, J. Solid State Chem. 7 (1973) 49–54.
[24] Anne Utzolino, Karsten Bluhm, Zur Synthese und Kristallstruktur von manganhaltigen Boratoxiden: $MnFe(BO_3)O$ und $MnAl_{0.5}Y_{0.5}(BO_3)O$, Z. Naturforsch. 50b (1995) 1146–1150.
[25] M.S. Platunov, N.V. Kazak, Yu.V. Knyazev, L.N. Bezmaternykh, E.M. Moshkina, A.L. Trigub, A.A. Veligzhanin, Y.V. Zubavichus, L.A. Solovyov, D.A. Velikanov, S. G. Ovchinnikov, Effect of Fe-substitution on the structure and magnetism in single crystals $Mn_{2-x}Fe_xBO_4$, J. Cryst. Growth 475 (2017) 239–246.
[26] A. Wiedenmann, P. Burlet, R. Chevalier, Mössbauer study of imperfect one dimensional magnetic systems $FeMgBO_4$ and $FeMg_2BO_5$, J. Magn. Magn. Mater. 15 (1980) 216–218.
[27] Yu.V. Knyazev, N.B. Ivanova, N.V. Kazak, M.S. Platunov, L.N. Bezmaternykh, D. A. Velikanov, A.D. Vasiliev, S.G. Ovchinnikov, G.Yu. Yurkin, Crystal structure and magnetic properties of Mn substituted ludwigite $Co_3O_2BO_3$, J. Magn. Magn. Mater. 324 (2012) 923–927.
[28] A.F.J. Morgownik, J.A. Mydosh, High-temperature susceptibility of the Cu Mn spin-glass, Phys. Rev. B 24 (9) (1981) 5277.
[29] K.V. Rao, M. Fähnle, E. Figueroa, O. Beckman, L. Hedman, Deviations from Curie-Weiss behavior in spin-glasses, Phys. Rev. B 27 (5) (1983) 3104.
[30] J.A. Mydosh, Spin-Glasses: An Experimental Introduction, Taylor & Francis, London, Washington, 1993.
[31] J. Souletie, J.L. Tholence, Critical slowing down in spin glasses and other glasses: Fulcher versus power law, Phys. Rev. B 32 (1) (1985) 516.
[32] Y. Bitla, S.N. Kaul, L.F. Barquín, Nonlinear susceptibilities as a probe to unambiguously distinguish between canonical and cluster spin glasses, Phys. Rev. B 094405 (2012).
[33] J.E. Hirsch, J.V. Jose, Low-temperature thermodynamic properties of a random Heisenberg antiferromagnetic chain (S = 1/2), J. Phys. C: Solid State Phys. 13 (3) (1980) L53.
[34] J.E. Hirsch, Low-temperature thermodynamic properties of a random anisotropic antiferromagnetic chain, Phys. Rev. B 22 (11) (1980) 5355.